Raman analysis of bilayer graphene film prepared on commercial Cu(0.5 at% Ni) foil

M.J. Madito[a], A. Bello[a], J.K. Dangbegnon[a], C.J. Oliphant[b], W.A. Jordaan[b], T.M. Masikhwa[a], D.Y. Momodu[a] and N. Manyala[a*]

[a]Department of Physics, Institute of Applied Materials, SARCHI Chair in Carbon Technology and Materials, University of Pretoria, Pretoria 0028, South Africa.

[b]National Metrology Institute of South Africa, Private Bag X34, Lynwood Ridge, Pretoria 0040, South Africa

Abstract

This study reports the Raman analysis of bilayer graphene films prepared on commercial dilute Cu(0.5 at% Ni) foils using atmospheric pressure chemical vapour deposition (AP-CVD). A bilayer graphene film obtained on Cu foil is known to have small-areas of bilayer (islands) with a significant fraction of non-Bernal stacking while that obtained on Cu/Ni is known to grow over a large-area with Bernal stacking. In the Raman optical microscope images, a wafer-scale monolayer and large-area bilayer graphene films were distinguished and confirmed with Raman spectra intensities ratios of 2D to G peaks. The large-area part of bilayer graphene film obtained was assisted by Ni surface segregation since Ni has higher methane decomposition rate and carbon solubility compared to Cu. The Raman data suggest a Bernal stacking order in the prepared bilayer graphene film. A four-point probe sheet resistance of graphene films confirmed a bilayer graphene film sheet resistance distinguished from that of monolayer graphene. A relatively higher Ni surface concentration in Cu(0.5 at% Ni) foil was confirmed with time-of-flight secondary ion mass spectrometry. The inhomogeneous distribution of Ni in a foil and the diverse crystallographic surface of a foil (confirmed with proton-induced X-ray emission (PIXE) and electron backscatter diffraction respectively), could be a reason for incomplete wafer-scale bilayer graphene film. The Ni surface segregation in dilute Cu(0.5 at% Ni) foil has a potential to impact on AP-CVD growth of large-area bilayer graphene film.

Keywords: Graphene Raman, Ni segregation, Cu(Ni) foil, AP-CVD graphene

---

[*] Corresponding Author: Tel: +27 (0)12 420 3549 and E-mail address: ncholu.manyala@up.ac.za (N. Manyala)

1. Introduction

Graphene (a two-dimensional crystalline form of carbon) due to its remarkable unique properties holds great promise for nanoscale electronics and photonics. However, graphene has no bandgap and that greatly limits its uses in electronics[1–3]. Interestingly, bilayer graphene with zero band gap behaves like a metal and if the mirror-like symmetry of the two layers is disturbed (to give Bernal (AB) stacked bilayer graphene), then behaves like a semiconductor[3]. Studies have engineered a bandgap in graphene, bilayer graphene, in particular, that can be controlled up to 250 meV by applying a perpendicular electric field[1–4]. One of the approaches of growing a Bernal-stacked bilayer graphene is by chemical vapour deposition (CVD) method. The CVD approach has demonstrated an excellent capability of growing wafer-scale high-quality AB-stacked bilayer graphene[5–8]. In CVD graphene growth, copper (Cu) is the most favorable substrate since it has lower carbon solubility (i.e. <0.001 at% at 1000 °C) and slow decomposition rate of methane (CH_4)[9]. Graphene growth on Cu surface is catalytic processes where hydrocarbon is decomposed in the formation of carbon atoms that initially aggregate and materialize into graphene film. The lower decomposition rate of methane by Cu is advantageous for wafer-scale monolayer graphene growth, but disadvantageous for wafer-scale bilayer graphene growth as it requires more carbon atoms. In fact, it is practically impossible to supply sufficient carbon atoms for wafer-scale multilayer graphene growth on pure Cu surface[5–15]. Generally, a bilayer graphene obtained on pure Cu foil is known to be incomplete (have smaller areas of bilayer) with a significant fraction of non-AB stacking[16–21].

Liu et al.[22] have shown with Cu/Ni films having a surface layer composition of about 97 at% Cu and 3 at% Ni, that the lower decomposition rate of CH_4 by Cu can be enhanced by Ni (which is known to have higher carbon solubility (i.e. ~1.3 at% at 1000 °C) and decomposition rate of CH_4[23]) to grow a wafer-scale AB-stacked bilayer graphene in CVD. Preparation of such Cu/Ni films on SiO_2/Si substrates requires an extra experimental procedure (such as SiO_2/Si substrates cleaning/preparation, thickness controllable thin films deposition and annealing for thin layers interdiffusion) compare to commercially available Cu-Ni foil. However, such Cu-Ni foil at CVD graphene growth temperatures in the range of 900-1000 °C should have surface layer composition of about 97 at% Cu and 3 at% Ni to grow wafer-scale AB stack bilayer graphene in accordance with results in reference 22.

In this study, we propose the use of homogeneous dilute Cu(0.5 at% Ni) foil which demonstrates surface layer composition of about 97 at% Cu and 3 at% Ni in the temperature range of 920-1000 °C; calculated using surface segregation models[24,25] described in the supporting information. The use of homogeneous dilute Cu(Ni) foil has rarely been studied for the CVD bilayer graphene growth. The objective of this study is to grow a large-area or wafer/scale high-quality bilayer graphene films on dilute Cu(0.5 at% Ni) foil using atmospheric pressure chemical vapour deposition (AP-CVD). The Raman data showed the capability of a dilute Cu(0.5 at% Ni) foil for growing a large-area bilayer graphene film. This capability of a dilute Cu(0.5 at% Ni) foil was ascribed primarily to the surface segregation of Ni in dilute Cu(0.5 at% Ni) foil (confirmed with time-of-flight secondary ion mass spectrometry) since Ni has higher methane decomposition rate and carbon solubility compare to Cu. The Raman data suggest a Bernal stacking order in the prepared bilayer graphene film. A prepared bilayer graphene film has a sheet resistance of 288 Ω/sqr.

2. Experimental

High purity (99.9 %) dilute Cu(0.5 at% Ni) foil samples (20 × 20 mm^2 and 0.5 mm thick) were ordered from MaTeck (package list No. 14040413-860). Samples were electro-polished and cleaned for graphene growth as follows: In the electrochemistry cell, the Cu(0.5 at% Ni) foil sample (to be polished) was connected to the anode and a Cu plate (30 mm in diameter and 2 mm thick) to the cathode of the cell and the electro-polishing solution was 1000 mL of water, 500 mL of ortho-phosphoric acid, 500 mL of ethanol, 100 mL of isopropyl alcohol, and 10 g of urea. A DC power supply was used to supply constant voltage/current in the electrochemistry cell and a voltage in the range of 3.0-6.0 V was applied for about 3 min. After electropolishing, the Cu(0.5 at% Ni) foils were rinsed with deionized water and immersed in aqueous nitric acid for 30 s to dissolve off the electro-polishing solution residues on the foil surface, then again in deionized water followed by ultra-sonic bath with acetone and isopropanol and dry-blowing with N_2 to remove water residues. After cleaning, Cu(0.5 at% Ni) foils were loaded in AP-CVD quartz tube setup for monolayer graphene and bilayer graphene growth successively. Samples were annealed under Ar (300 sccm) and H_2 (9 sccm) flow for 30 min at 1050 °C before the growth of graphene. After annealing, a monolayer graphene was synthesized from a mixture of gases, Ar (300 sccm): H_2 (9 sccm): CH_4 (15 sccm) and a bilayer graphene from a mixture of Ar (300 sccm): H_2 (9 sccm): CH_4 (10 sccm) at 980 °C for exactly 9 min. Immediately after growth, the CH_4 flow was stopped and the quartz tube was pushed to the cooler region of the furnace and samples rapidly cooled down to room temperature and off loaded from AP-CVD quartz tube.

The graphene films were transferred onto 300 nm thick SiO_2/Si substrates. In the transfer, a thin layer of polymethyl methacrylate (PMMA) (average Mw ~996 000 by GPC) dissolved in chlorobenzene with a concentration of 46 mg/mL was spin-coated on the as-grown graphene films on Cu(0.5 at% Ni) foils at 3000 rpm for 30 s. PMMA deposited on graphene films/Cu(0.5 at% Ni) foils was cured at 115 °C for 5 min. PMMA/graphene/ Cu(0.5 at% Ni) foil samples were placed in 1 M iron nitrate to etch off Cu and transferred using a polyethylene terephthalate (PET) to the 5% hydrochloride (HCl) and deionized water to dissolve the iron nitrate, and then onto SiO_2 substrates. Finally, PMMA was removed using acetone.

Graphene/SiO_2/Si samples (graphene films) were characterized with Raman spectroscopy (WITec Alpha 300 micro-Raman imaging system with 532 nm excitation laser). Raman spectra were measured at room temperature with the laser power set below 2 mW in order to minimize heating effects. The graphene films sheet resistance measurements were carried out in ambient conditions (i.e. in air at room temperature and pressure) using a Signatone four point probe station. A Cu(0.5 at% Ni) foil was analyzed with electron backscatter diffraction (EBSD) performed in a LEO 1525 field-emission gun scanning electron microscope (FEGSEM) at an acceleration voltage of 25 kV using the Oxford INCA crystal software. Proton-induced X-ray emission (PIXE) was used to map Ni distribution in Cu(0.5 at% Ni) foils. Time-of-flight secondary ion mass spectroscopy (TOF-SIMS) surface imaging (elemental map) of Cu(0.5 at% Ni) foils was performed using the TOF-SIMS5 Ion-TOF system. The mass spectra were calibrated to the following mass peaks in positive mode: Al, Na, Ni, Fe, Si, C, C_2H_5 K and Cu. The analysis was carried out over an area of 500 × 500 μm^2 and ion sputter gun area of 1000 × 1000 μm^2.

3. Results and discussions

In the Raman spectrum of graphene, the main features that are observable are the G-band mode (~1590 cm^{-1}), the 2D-band mode (~2690 cm^{-1}) and the D-band mode or the disorder-induced band (1350 cm^{-1})[1,21]. The G-band originates from a normal first-order Raman scattering process in graphene and involves the sp^2 hybridized carbon atoms of the graphene layer, the 2D-band from a second-order process that involves two in-plane transverse optical mode (iTO) phonons near the *K* point and the D-band from a second-order process that involves one iTO phonon and one defect[1,21]. The Raman process can also give rise to the triple-resonance Raman process which might explain a more intense 2D-band relative to the G-band in monolayer graphene[1]. By observing the differences in the 2D-band and the G-band intensity ratios, the 2D-band frequency (peak width) and line shape, the number of graphene layers contained in graphene films can be obtained and also the stacking order or interlayer interactions in few layers graphene films[1,21]. Figure 1(a) and (b) show the Raman optical microscope images (obtained using 100×/0.90 objective lens) of mono and bilayer graphene films transferred onto 300 nm thick SiO$_2$/Si substrates. Importantly, the optical microscope of graphene films displays the image color contrast between monolayer and multilayer graphene films hence it is used to distinguish between the two. The optical microscope image for monolayer graphene (Fig. 1(a)) shows a wafer-scale graphene film and for bilayer graphene film (Fig. 1(b)) shows large-area bilayer graphene (darker areas) with smaller-areas of monolayer graphene (lighter areas). Figure 1(c) shows the average Raman spectra obtained from 30 μm^2 areas of monolayer and bilayer graphene films shown in Fig. 1(a) and (b) with square boxes. The mapping of G peaks intensities of the obtained Raman spectra over 30 μm^2 areas of monolayer and bilayer graphene films are shown in Fig. S2 (Supporting information) and shows relative uniform intensity over an analyzed area. It can be seen in Fig. 1(c) that the G peaks intensities scale range for bilayer graphene is twice that for monolayer graphene (also see the G peaks intensities mapping in Fig. S2 (Supporting information)) and that shows a distinction between mono and bilayer graphene films. The G-band position can give insight into the number of layers present in the graphene film, however, it can be affected by film conditions such as temperature, doping, and small amounts of strain present in the film. Nonetheless, the G-band intensity which is less susceptible to such film conditions shows a behavior that follows a linear trend as the number of layers increases from mono to multilayer graphene[1,21,26,27]. In Fig. 1(c), the absence of the D-band (at ~ 1360 cm^{-1}) in Raman spectra demonstrates high-quality graphene since D-band appears due to the presence of impurities or defects in the translational symmetry of the carbon material's lattice[1,21,26,27]. A wafer-scale monolayer graphene obtained demonstrate a known capability of graphene of growing over grain boundaries and grains on polycrystalline Cu surface[26]. The smaller-areas of monolayer graphene present in prepared bilayer graphene demonstrate the physical challenge of supplying sufficient carbon atoms for wafer-scale multilayer graphene growth on Cu foil[4,28]. The challenge could be as a result of lower decomposition rate of methane by Cu (especially in Cu surface areas or grains where there is almost 0 at% Ni concentrations) and the diverse surface orientations present in Cu surface[29]. In addition, a similar bilayer graphene film was obtained (see the optical microscope image in Fig. S3 (Supporting information)) through the same experimental procedure on additional dilute Cu(0.5 at% Ni) foil sample which confirms the observed challenge of obtaining a wafer-scale bilayer graphene film on Cu.
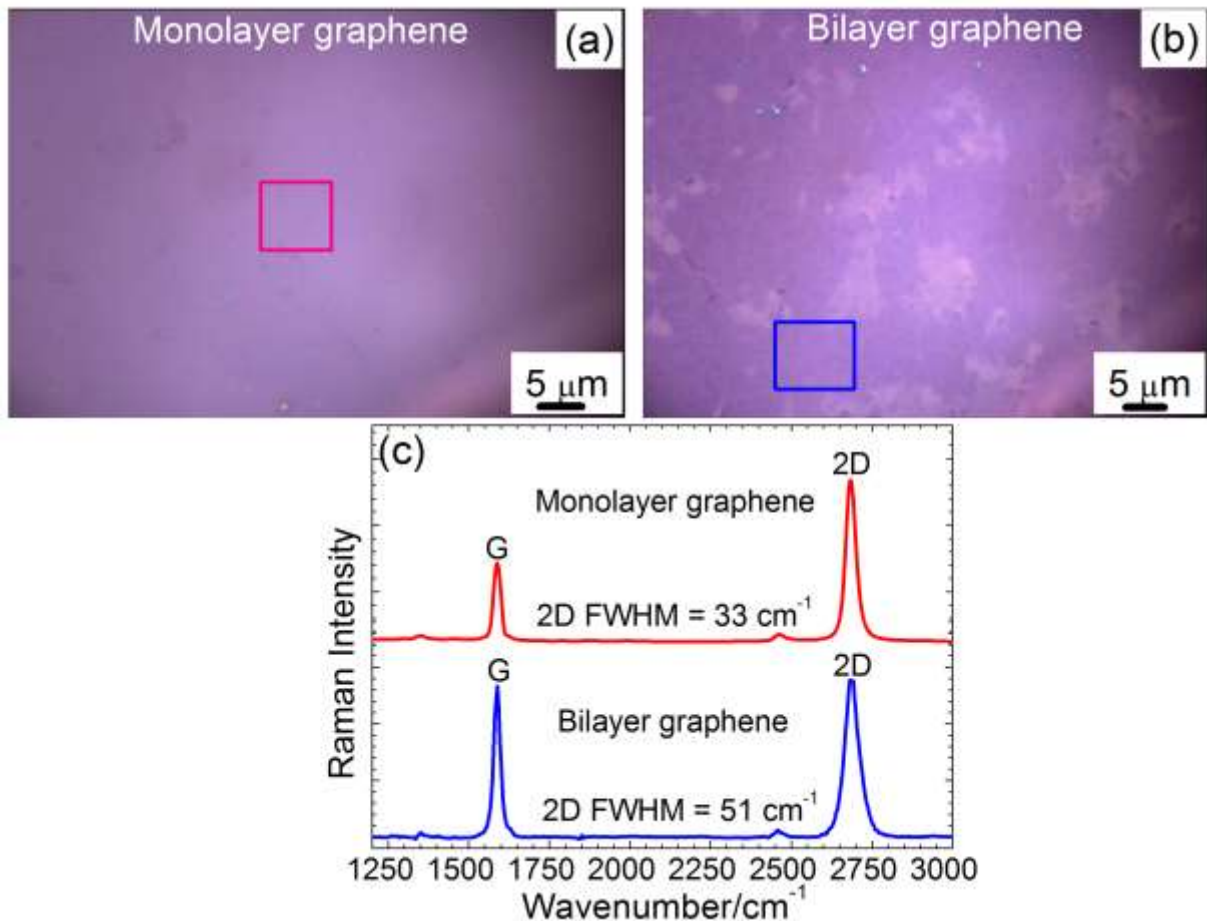
Figure 1. The Raman optical microscope images (obtained using 100×/0.90 objective lens) of (a) monolayer and (b) bilayer graphene films transferred onto 300-nm-thick SiO_2/Si substrates. (c) The average Raman spectra obtained from 30-μm^2 areas of monolayer and bilayer graphene films shown in (a) and (b) with square boxes.

Figure 2(a) and (b) show the mapping of 2D peaks Full width at half maximum (FWHM) and the corresponding 2D to G peaks intensities ratio (I_{2D}/I_G) mapping respectively, for monolayer and bilayer graphene films. For monolayer graphene the 2D peaks FWHMs are in the range of $26-38$ cm^{-1} and I_{2D}/I_G in the range of ~2.5−4.5, while for bilayer graphene the distribution of the FWHMs is in the range of $39-65$ cm^{-1} (with a cut-off FWHM of about 70 cm^{-1}) and I_{2D}/I_G in the range of 0.5−2.2. Figure 2 clearly demonstrates and distinguishes characteristics features of monolayer and bilayer graphene as expected.

In monolayer graphene, the 2D-band mode has a single Lorentzian feature[3]. In AB-stacked bilayer graphene, the electronic band split into two conduction and two valence bands. The upper (lower) and lower (upper) branches of the valence (conduction) band are referred to as π_1 (π_1^*) and π_2 (π_2^*) respectively, as illustrated with a schematic view in Fig. 3(a)[1,21,26,27]. Since 2D-band originates from second-order Raman process that involves two iTO phonons, the electronic band split causes splitting of the phonon bands into two components such that the electron–phonon scattering occurs with two phonons with symmetries T_1 and T_2[26]. For a T_1 phonon the scattering occurs between bands of the same symmetry (i.e. π_1 and π_1^* or π_2 and π_2^*) and for a T_2 phonon, the scattering occurs between bands of different symmetries (i.e.
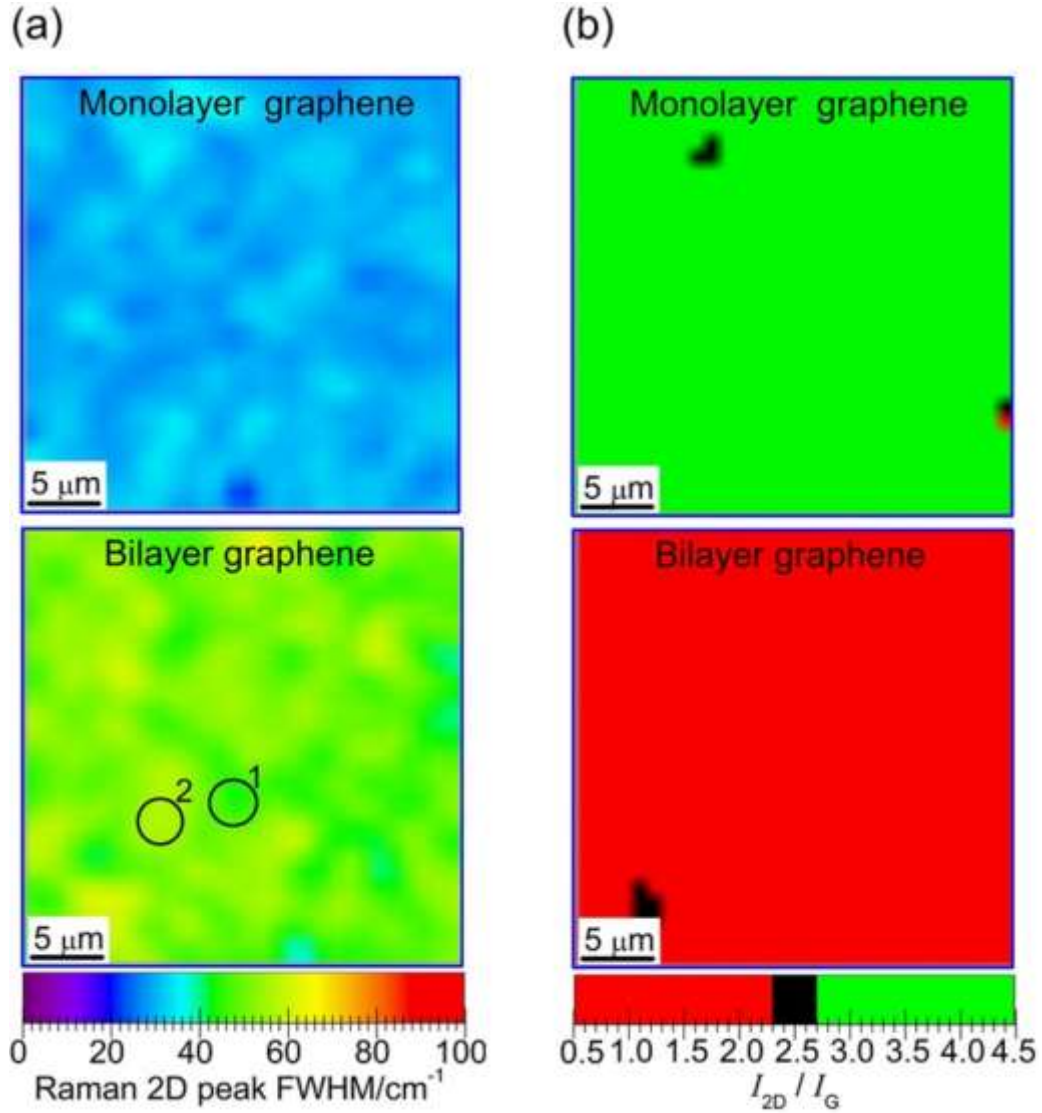
Figure 2. (a) The 2D peak full width at half maximum (FWHM) mapping and (b) the corresponding 2D to G peak intensities ratio (I_{2D}/I_G) mapping for monolayer and bilayer graphene films, respectively, transferred onto SiO$_2$/Si substrate (the data are the same, acquired from the 30-µm^2 area in Fig. 1).

π_1 and π_2^*). T_1 and T_2 phonon processes are labeled as P_{ij} (with the relative magnitudes of the four phonon wavevectors q), where i (j) denote an electron scattered from (to) each conduction band $\pi_{i(j)}^*$ (see Fig. 3(a) schematic view). The P_{11}, P_{22}, P_{12} and P_{21} scattering processes originating from an iTO phonon give rise to four peaks in the Raman 2D peak with peaks wavenumbers at approximately 2655, 2680, 2700, and 2725 cm^{-1} respectively and FWHMs equal that of monolayer graphene 2D peak[26]. These four peaks are fitted as four Lorentzians to 2D peak[1,21,26,27]. The amplitudes of the two Lorentzians at ~2680 and ~2700 cm^{-1} (inner peaks in 2D peak) have almost the same intensity and are higher than the other two at ~2655 and ~2725 cm^{-1} (outer peaks in 2D peak) as shown with a schematic view of these peaks in Fig. 3(a) (similar to Lorentzians usually obtained for exfoliated AB-stacked bilayer graphene)[26,27]. The amplitudes of the four Lorentzians depend on the laser energy which was maintained constant in this work. Figure 3(b) shows spectra 1 and 2 from circles 1 and 2 in Fig. 2(a) and the 2D peaks are fitted with four Lorentzians each with FWHM feature
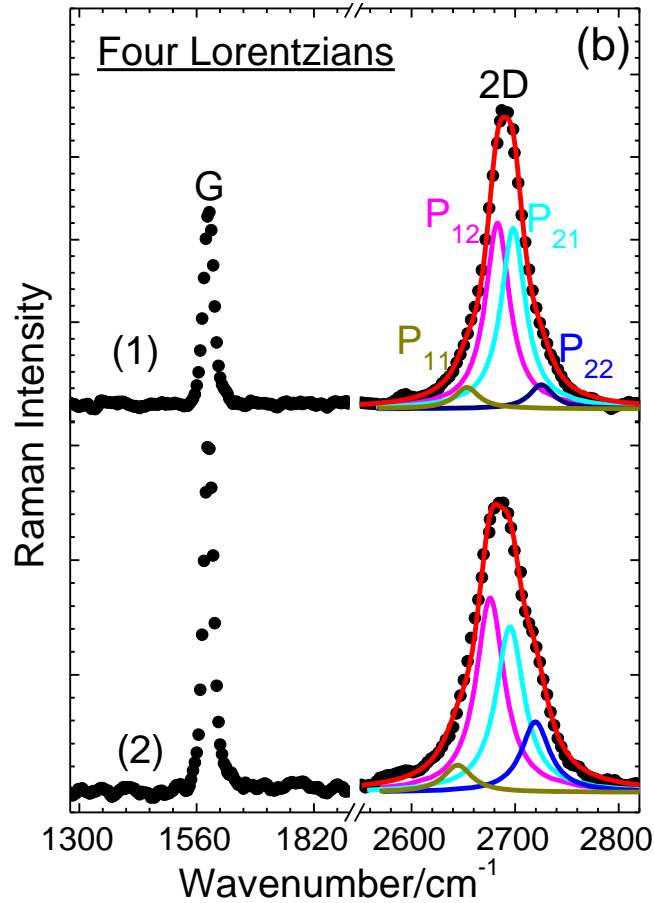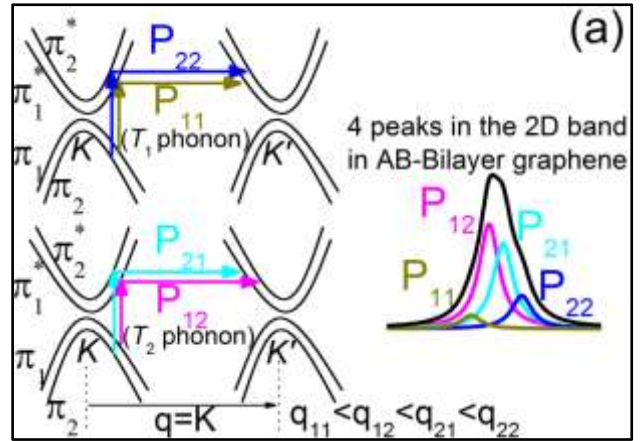
Figure 3. (a) Schematic view of the electron dispersion of bilayer graphene near the K and K' points showing both π_1 and π_2 bands. The resonance Raman processes due to electronic band split are indicated as P_{11}, P_{22}, P_{12} and P_{21} with the relative magnitudes of the four phonon wavevectors q.[1] (b) The Raman spectra from two different spots of bilayer graphene film [spectra 1 and 2 are from circles 1 and 2 in Fig. 2(a)] transferred onto SiO$_2$/Si substrate. The solid lines are Lorentzian fits of 2D peaks. AB, Bernal.

of a monolayer graphene. The four Lorentzians in Fig. 3(b) demonstrate characteristics of the AB-stacked bilayer graphene. To further investigate the possibility of large-area trilayer graphene, six Lorentzians fits were performed (Fig. S4 (Supporting information)) and only four of six Lorentzians fitted inside 2D peak, which further confirmed bilayer graphene in the

sample. In brief, the Raman spectroscopy/imaging confirm a large-area bilayer in prepared graphene film distinguished from monolayer graphene and suggest a Bernal stacking order in prepared bilayer graphene film. Of course, Raman spectroscopy/imaging is a well-known powerful and noninvasive technique to determine, among others, the number of graphene layers, the stacking order and the interlayer interactions in few layers graphene sample[26,27,30,31].
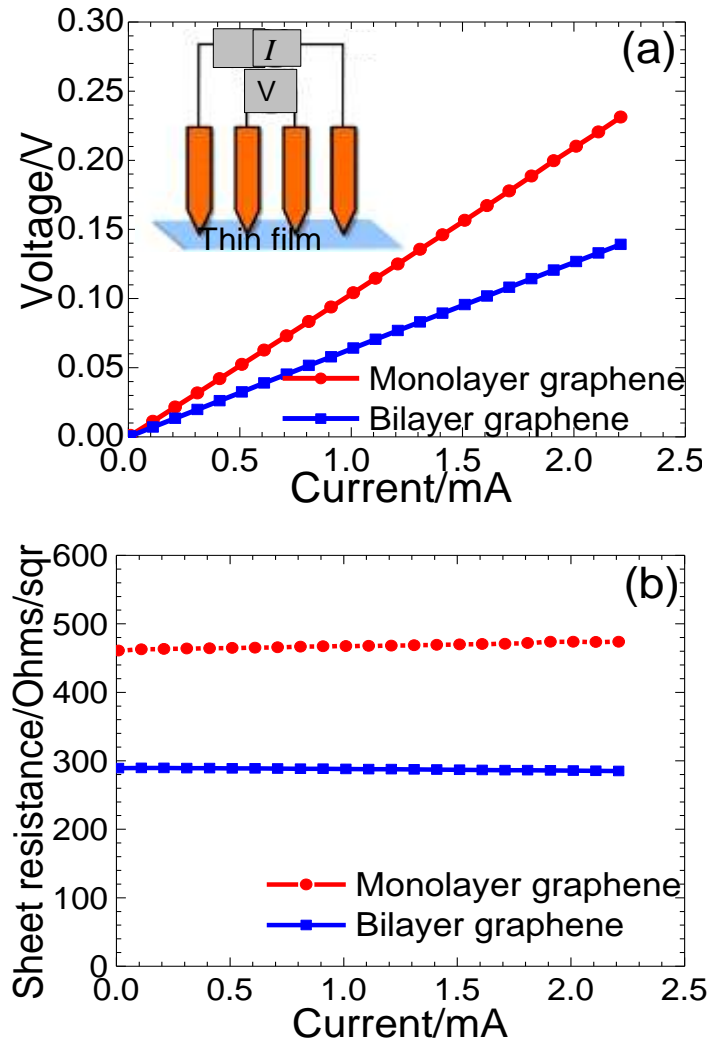

Figure 4. (a) A four-point probe-measured voltage drop for monolayer and bilayer graphene films transferred onto SiO$_2$/Si substrates (insert to figure shows a schematic that shows that in a four-point probe, two electrodes are used for sourcing a direct current, *I*, and the other two for measuring the corresponding voltage drop, *V*) and (b) the calculated sheet resistance of the corresponding graphene films.

Figure 4(a) shows the measured voltage drop for monolayer and bilayer graphene films which was used to calculate the sheet resistance of graphene films (Fig. 4(b)) using an approach which relies on a geometric factor. A monolayer graphene film has a high sheet resistance (468 Ω/sqr) compare to bilayer graphene film (288 Ω/sqr) since sheet resistance decreases with the increase in graphene film thickness (number of layers). The sheet resistance measured compares with those measured from a monolayer (409 Ω/sqr) and bilayer graphene (287 Ω/sqr) films in reference 18. The sheet resistance is determined by the

carrier density and mobility[32]. For instance, at low temperatures (~4 K) a monolayer graphene with high sheet resistance has a high Hall mobility with low carrier density[33]. In contrary, a bilayer graphene with low sheet resistance has a high Hall mobility and high carrier density[33]. These properties are used to distinguish monolayer and bilayer graphene and are ascribed to different band structures and scattering mechanisms in these layers of graphene[3,33,34]. Therefore, the sheet resistance shows a strong dependence of the electrical prosperities on graphene film thickness, primarily relate to the interlayer coupling[33,34]. These measurements of the carrier transport properties of graphene were not performed in this work.
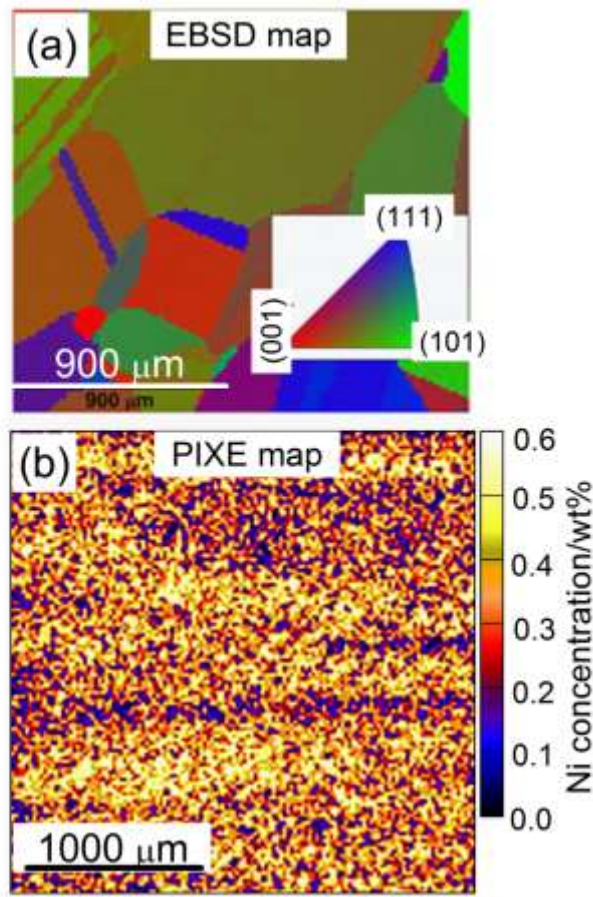
Figure 5. (a) Electron backscatter diffraction (EBSD) map of the annealed Cu(0.5 at% Ni) foil surface, and the inset to the figure is the corresponding inverse pole figure orientation component coloring scheme. (b) Proton-induced X-ray emission (PIXE) map of Ni distribution in the annealed Cu(0.5 at% Ni) foil.

Figure 5(a) and (b) show EBSD and PIXE mapping of the grains surface orientations of the annealed Cu(0.5 at% Ni) foil surface (with an average grain size of 116 μm) and Ni concentration distribution in the annealed Cu(0.5 at% Ni) foil respectively. An EBSD map shows a crystallographic diverse surface of Cu(0.5 at% Ni) foil, composed of terraces of low index Cu planes (111), (101) and (001) and larger intermediate planes in accordance with the inverse pole figure orientation component coloring scheme (inset to figure). In CVD graphene growth on Cu foil, only the surface of a foil is important since the growth is limited to surface reaction. It is known that the surface crystallography of the Cu foil influences the CVD graphene growth rate. High index Cu planes cause compact graphene island formation with growth rates faster than those on Cu(100)[18,33]. A Cu(111) plane also has fast growth

rate, but grows monolayer graphene and influences nearby growth dynamics[33]. Meaning, graphene growth on the Cu(111) surface grows over grain boundaries into the adjacent high index Cu surfaces. Therefore, traces of Cu (111) surface in Cu(0.5 at% Ni) foil led to smaller-areas of monolayer graphene present in prepared bilayer graphene. A PIXE map for Cu(0.5 at% Ni) foil shows inhomogeneous distribution and high Ni concentration of 0.5 at%, as expected. Inhomogeneous distribution of Ni could be due to grain boundaries, different grains (orientations) and the presence of other impurities in the foil which most likely compete with Ni for lattice sites. An observed inhomogeneous distribution of Ni in foil bulk will also be observed in the surface due to grain boundaries and different grains surface orientations. For instance, low energy electron diffraction over-structures have shown that the maximum surface concentration of a substitutional segregating element for Cu(001), Cu(101) and Cu(111) is 25, 50 and 33 at% respectively[25,36]. High Ni surface concentrations will cause faster methane decomposition and graphene growth rate as compared to surfaces with low Ni concentrations. Therefore, inhomogeneous distribution of Ni in Cu foil surface will contribute differently to graphene growth rates on different grains surfaces.
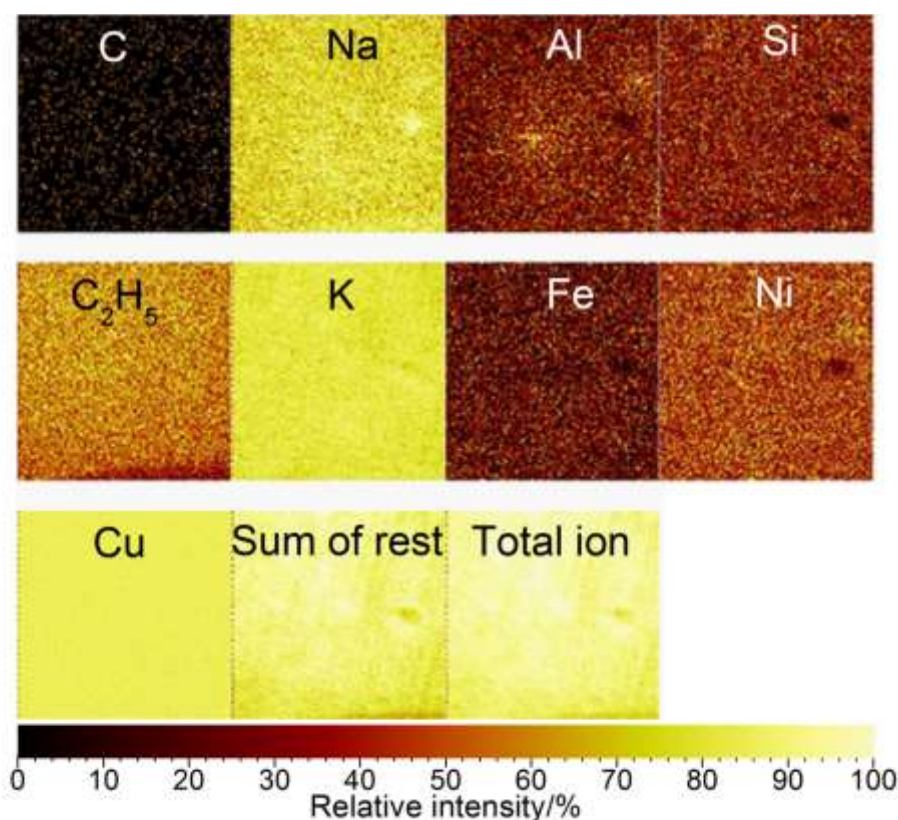
Figure 6. The map images of time-of-flight secondary ion mass spectroscopy secondary ion intensities measured from a dilute Cu(0.5 at% Ni) surface before surface cleaning with ion sputtering.

Figure 6 shows the map images of TOF-SIMS secondary ion intensities measured from a dilute Cu(0.5 at% Ni) surface (i.e. after annealing under graphene growth conditions without methane source) before surface cleaning (and after surface cleaning for 180 s with ion sputtering see Fig. S5 (Supporting information)). Figure 6 shows high surface concentrations (or relative intensities) of Al, Na, Ni, Fe, Si, C_2H_5 and K in Cu(0.5 at% Ni) foil which result

from impurities segregation. Impurities of Cu surface play a critical role in determining the number of graphene layers during CVD graphene growth, but the effect of each impurity is determined by a metal-carbon atomic interaction energy, metal-methane decomposition rate and metal-carbon solubility. Though, Na and K alkali-metals (and C_2H_5) show high relative intensities at room temperature they will not dominate the surface during CVD growth at high temperature of 980 °C due to their very low melting points (< 100 °C). Compare to other elements, high relative intensities of Na and K in foil do not necessarily show high surface concentrations of these elements since they have strong signals in TOF-SIMS. Al, Si and Fe impurities have bulk concentrations in the order of few parts per million (ppm) compare to Ni which has 5000 ppm (0.5 at%) and hence Ni has higher surface concentration (Fig. 6). Compare to these impurities, after surface cleaning with ion sputtering (Fig. S5 (Supporting information)) Ni has higher bulk concentration as expected. Amongst impurities detected in the foil surface, Ni has strong carbon-metal atomic interaction, high methane decomposition rate, high carbon solubility and high bulk concentration (which act as Ni supplier to reach high Ni surface concentrations)[1,21,26,37]. As a result, surface Ni will contribute significantly during CVD graphene growth on Cu(0.5 at% Ni) foil.

Furthermore, the thermodynamically driven segregation of Ni in dilute Cu(0.5 at% Ni) foil can be described according to Darken description (surface segregation model) which state that segregation of impurities in dilute alloy is driven by a change in chemical potential energy which results in the minimization of the total energy of the crystal[25]. Using surface segregation models it can be shown that at a growth temperature of 980 °C, the Ni surface concentration is X_{Ni}^{S} = 2.1, 1.4 and 1.1 at% for Cu(001), Cu(111) and Cu(101) surfaces respectively (see the calculation of Fig. S1 (Supporting information)). Therefore, at 980 °C, a surface layer of a dilute Cu(0.5 at% Ni) foil will have about 1.5 at% Ni on average and the impurities with bulk concentrations in the order of few ppm will have < 0.01 at% surface concentrations. Once more, Liu et al.[22], using Cu/Ni thin films with a surface layer consisting of > 97 at% Cu and < 3 at% Ni have produced a large-area AB-stacked bilayer graphene film. Similarly, a dilute Cu(0.5 at% Ni) foil has produced a large-area bilayer graphene film which is suggested to be AB-stacked according to Raman data. The processes such as segregation from grains and grain boundaries and the segregation dependence of different grains surfaces play a role in surface concentration build-up of segregating impurity. Therefore, in a polycrystalline foil which has crystallographic diverse surface it is difficult to control or separate these contributions from each other (even in the calculation using surface segregation models). Therefore, the Ni surface concentration calculated using surface segregation models approximates to an actual average Ni surface concentration expected in dilute Cu(0.5 at% Ni) foil at a growth temperature of 980 °C.

4. Conclusions

In this study, the Raman analysis of graphene films prepared on commercial dilute Cu(0.5 at% Ni) foils using AP-CVD are reported. The AP-CVD growth of graphene films focused on growing a large-area AB stacked bilayer graphene film. In the Raman optical microscope images, a wafer-scale monolayer and large-area bilayer graphene films were distinguished and confirmed with Raman spectra data. The Raman data suggest a Bernal stacking order in prepared bilayer graphene film. A four-point probe sheet resistance of graphene films confirmed a bilayer graphene film sheet resistance distinguished from that of monolayer graphene. The large-area part of bilayer graphene film obtained on dilute Cu(0.5 at% Ni) foil was assisted by Ni surface concentration since Ni has higher methane

decomposition rate and carbon solubility as compared to Cu. A relatively higher Ni surface concentration in Cu(0.5 at% Ni) foil was confirmed with time-of-flight secondary ion mass spectrometry. The inhomogeneous distribution of Ni in a foil and the diverse crystallographic surface of a foil (confirmed with Proton-induced X-ray emission and electron backscatter diffraction respectively), could be a reason for incomplete wafer-scale bilayer graphene film. Since, high index Cu planes and low index Cu(001), Cu(101) planes are known to grow compact graphene and Cu(111) plane to grow monolayer graphene which grows over grain boundaries into the adjacent grains. Though, we propose a homogeneous dilute Cu(0.5 at% Ni) foil, we also suggest that a foil should consist of low index Cu(001) or Cu(101) surfaces to archive a wafer-scale AB stacked bilayer graphene film in AP-CVD.

Acknowledgements

References

[1]   Y. Zhang, T.-T. Tang, C. Girit, Z. Hao, M. C. Martin, A. Zettl, M. F. Crommie, Y. R. Shen, F. Wang, *Nature* **2009**, *459*, 820.

[2]   W. J. Yu, L. Liao, S. H. Chae, Y. H. Lee, X. Duan, *Nano Lett.* **2011**, *11*, 4759.

[3]   H. Aoki, Mildred S. Dresselhaus, Eds. , *Physics of Graphene*, Springer, New York, **2014**.

[4]   W. Liu, H. Li, C. Xu, Y. Khatami, K. Banerjee, *Carbon N. Y.* **2011**, *49*, 4122.

[5]   S. Bhaviripudi, X. Jia, M. S. Dresselhaus, J. Kong, *Nano Lett.* **2010**, *10*, 4128.

[6]   I. Vlassiouk, M. Regmi, P. Fulvio, S. Dai, P. Datskos, G. Eres, S. Smirnov, *ACS Nano* **2011**, *5*, 6069.

[7]   H. Kim, E. Saiz, M. Chhowalla, C. Mattevi, *New J. Phys.* **2013**, *15*, 053012.

[8]   A. W. Robertson, J. H. Warner, *Nano Lett.* **2011**, *11*, 1182.

[9]   G. A. López, E. J. Mittemeijer, *Scr. Mater.* **2004**, *51*, 1.

[10]   Q. Li, H. Chou, J. H. Zhong, J. Y. Liu, A. Dolocan, J. Zhang, Y. Zhou, R. S. Ruoff, S. Chen, W. Cai, *Nano Lett.* **2013**, *13*, 486.

[11]   S. Nie, W. Wu, S. Xing, Q. Yu, J. Bao, S. Pei, K. F. McCarty, *New J. Phys.* **2012**, *14*, 093028.

[12]   M. Fabiane, S. Khamlich, A. Bello, J. Dangbegnon, D. Momodu, A. T. Charlie Johnson, N. Manyala, *AIP Adv.* **2013**, *3*, 112126.

[13]   K. Yan, H. Peng, Y. Zhou, H. Li, Z. Liu, *Nano Lett.* **2011**, *11*, 1106.

[14]   B. Wu, D. Geng, Y. Guo, L. Huang, Y. Xue, J. Zheng, J. Chen, G. Yu, Y. Liu, L. Jiang, W. Hu, *Adv. Mater.* **2011**, *23*, 3522.

[15]   P. Wu, X. Zhai, Z. Li, J. Yang, *J. Phys. Chem. C* **2014**, *118*, 6201.

[16]   N. Liu, L. Fu, B. Dai, K. Yan, X. Liu, R. Zhao, Y. Zhang, Z. Liu, *Nano Lett.* **2011**, *11*, 297.

[17]   A. Reina, X. Jia, J. Ho, D. Nezich, H. Son, V. Bulovic, M. S. Dresselhaus, J. Kong, *Nano Lett.* **2009**, *9*, 30.

[18]   S. Chen, W. Cai, R. D. Piner, J. W. Suk, Y. Wu, Y. Ren, J. Kang, R. S. Ruoff, *Nano Lett.* **2011**, *11*, 3519.

[19]   X. Liu, L. Fu, N. Liu, T. Gao, Y. Zhang, L. Liao, Z. Liu, *J. Phys. Chem. C* **2011**, *115*, 11976.

[20]   Y. Wu, H. Chou, H. Ji, Q. Wu, S. Chen, W. Jiang, Y. Hao, J. Kang, Y. Ren, R. D. Piner, R. S. Ruoff, *ACS Nano* **2012**, *6*, 7731.

[21]   W. Fang, A. L. Hsu, R. Caudillo, Y. Song, a. G. Birdwell, E. Zakar, M. Kalbac, M. Dubey, T. Palacios, M. S. Dresselhaus, P. T. Araujo, J. Kong, *Nano Lett.* **2013**, *13*, 1541.

[22]   W. Liu, S. Kraemer, D. Sarkar, H. Li, P. M. Ajayan, K. Banerjee, *Chem. Mater.* **2014**, *26*, 907.

[23]   W. Cai, R. D. Piner, Y. Zhu, X. Li, Z. Tan, H. C. Floresca, C. Yang, L. Lu, M. J. Kim, R. S. Ruoff, *Nano Res.* **2009**, *2*, 851.

[24]   E. C. Viljoen, J. du Plessis, *Surf. Sci.* **1999**, *431*, 128.

[25]   J. du Plessis, *Solid State Phenomena - Part B, Volume 11 (Diffusion and Defect Data)*, Sci-Tech Publications, Brookfield USA, **1990**.

[26]   A. C. Ferrari, J. C. Meyer, V. Scardaci, C. Casiraghi, M. Lazzeri, F. Mauri, S. Piscanec, D. Jiang, K. S. Novoselov, S. Roth, A. K. Geim, *Phys. Rev. Lett.* **2006**, *97*, 187401.

[27]   L. M. Malard, M. a. Pimenta, G. Dresselhaus, M. S. Dresselhaus, *Phys. Rep.* **2009**, *473*, 51.

[28]   A. Guermoune, T. Chari, F. Popescu, S. S. Sabri, J. Guillemette, H. S. Skulason, T. Szkopek, M. Siaj, *Carbon N. Y.* **2011**, *49*, 4204.

[29]   J. D. Wood, S. W. Schmucker, A. S. Lyons, E. Pop, J. W. Lyding, *Nano Lett.* **2011**, *11*, 4547.

[30]   J. M. Caridad, F. Rossella, V. Bellani, M. S. Grandi, E. Diez, *J. Raman Spectrosc.* **2011**, *42*, 286.

[31]   J. M. Caridad, F. Rossella, V. Bellani, M. Maicas, M. Patrini, E. Díez, *J. Appl. Phys.* **2010**, *108*, 084321.

[32]   Y. Liu, W. Li, M. Qi, X. Li, Y. Zhou, Z. Ren, *Phys. E Low-dimensional Syst. Nanostructures* **2015**, *69*, 115.

[33]   W. Zhu, V. Perebeinos, M. Freitag, P. Avouris, *Phys. Rev. B* **2009**, *80*, 235402.

[34]   C. Cobaleda, E. Diez, M. Amado, S. Pezzini, F. Rossella, V. Bellani, D. López-Romero, D. K. Maude, *J. Phys. Conf. Ser.* **2013**, *456*, 012006.

[35]   E. C. Viljoen, J. du Plessis, *Surf. Sci.* **1999**, *431*, 128.

[36]   E. C. Viljoen, J. du Plessis, *Surf. Sci.* **2000**, *468*, 27.

[37]   A. Dahal, M. Batzill, *Nanoscale* **2014**, *6*, 2548.